View metadata, citation and similar papers at core.ac.uk
brought to you by CORE
provided by UPCommons. Portal del coneixement obert de la UPC

XIV International Conference on Computational Plasticity. Fundamentals and Applications
COMPLAS 2019
E. Oñate, D.R.J. Owen, D. Peric , M. Chiumenti, and Eduardo de Souza Neto (Eds)

PLASTIC DISLOCATION AND INCOMPATIBILITY DENSITY AS INDICATORS FOR RESIDUAL STRESSES

PHILIPP LANDKAMMER*, PAUL STEINMANN*

* Institute for Applied Mechanics (LTM)
Friedrich-Alexander-Universität Erlangen-Nürnberg (FAU)
Egerlandstrasse 5, 91058 Erlangen, Germany
e-mail: philipp.landkammer@fau.de, paul.steinmann@fau.de, www.ltm.tf.fau.de

Key words: Incompatibility Density, Residual Stresses, Differential Geometry.

Abstract. Residual stresses in forming simulations are typically investigated by analyzing the remaining stress state after removing all external loadings. However, the generation of the stress state during forming remains unknown. As a remedy, we use the plastic and elastic dislocation and incompatibility densities - derived from continuum mechanical and differential geometrical considerations - as indicators to track the generation of residual stresses through out a forming operation. Theoretical backgrounds for small and large strain plasticity are highlighted and practical aspects regarding implementation are provided. Two examples demonstrate the functionality of the approach, whereby the plastic incompatibility density in phenomenological, multiplicative large strain plasticity serves as indicator.

1 INTRODUCTION

During a forming process, residual stresses occur in the manufactured components. In general, these have a decisive influence on their forming, application and failure behaviour. Regarding a workpiece under cyclic bending, compressive residual stresses close to the surface of the workpiece improve its life-time behaviour, whereas tensile residual stresses promote crack initialization. In particular within cold extrusion processes, high residual stresses occur due to the required forming forces. Thereby, a number of forming experiments have been used to investigate the dependencies of residual stresses on contact and friction conditions and geometry changes, see [1] among others. However, a deeper understanding of residual stresses is required to explore the total potential of deliberately influencing the workpiece behaviour through forming-induced residual stresses.

As a common definition, stresses which remain in the component after removing all external loadings are denoted as residual stresses. Therefore, the numerical investigation of residual stresses within the framework of a finite element (FE) simulation is typically based on the quantification and visualization of the remaining stress state within the unloaded component at the end of a forming operation. However, residual stresses arise during the whole forming process, and possibly also reduce again in case of an opposite load application. Since the residual stress generation during forming is not yet captured in the conventional procedure, a post-processing technique for an accompanying tracking of residual stresses would be of major interest to control them within manufacturing.

From a mechanical point of view, incompatible plastic strains in case of an inhomogeneous plastic deformation are responsible for residual stresses. In more detail, residual stresses arise in consequence of elastic lattice distortions, which are required to ensure that no gaps or overlaps occur despite the underlying incompatible plastic strains. By using differential geometrical considerations, Kröner [2] developed a linear continuum theory for residual strains with respect to additive small strain plasticity and further extended the approach also to nonlinearities [3]. For instance, a second order incompatibility density tensor is introduced therein to quantify the incompatible plastic strains.

Our idea is to use the dislocation and incompatibility densities as indicators for residual stresses. The theoretical aspects are transferred even to multiplicative large strain plasticity in [4], which provides the applicability of these indicators also to forming simulations.

The paper is structured as follows: Section 2 provides an overview to classify incompatible plastic strains within plastic deformations. Section 3 reiterates the computation of plastic incompatibilities in small strain plasticity and also recaptures its extension to multiplicative large strain plasticity. The functionality of these indicator for residual stresses is demonstrated by the plastic incompatibility density for two examples of a homogeneous and an inhomogeneous plastic deformation in Section 4. Finally, Section 5 summarizes the findings.

2 MECHANICAL VIEW ON RESIDUAL STRAINS

The theory of crystal plasticity is fundamental for describing the generation of residual stresses. Macroscopically observed plastic deformations within a forming process are the result of dislocation flow at the microscale. Thereby, dislocations partially get stucked within the periodically arranged crystal lattice and remain as additional obstacles for further dislocations flow, which leads to plastic hardening.

As illustrated by the diagram in **Figure 1**, a classification of plastic deformations according to the generated dislocation structure is stated as follows: Homogeneous plastic deformations lead purely to the formation of so-called statistically stored dislocations (SSD), which are responsible for plastic hardening. In case of inhomogeneous plastic deformations, geometrically necessary dislocations (GND) are generated in addition. They are responsible for maintaining the inhomogeneous plastic deformation after removing all external loadings [5]. GNDs are further distinguished, whether they cause macroscopically stress-free lattice curvatures or lead to incompatible plastic strains. Incompatible plastic strains induce incompatible elastic strains as their counterparts to guarantee the continuity of the continuum. These elastic residual strains cause residual stresses.

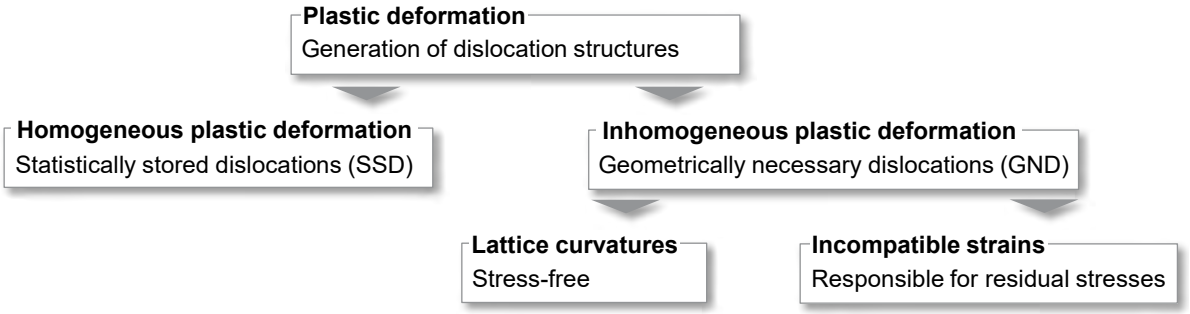

Figure 1: Incompatible strains in case of an inhomogeneous plastic deformation cause residual stresses

3 COMPUTATION OF DISLOCATION AND INCOMPATIBILTY DENSITIES

Concepts of differential geometry and continuum mechanics allow to describe the classification of plastic deformations as depicted in **Figure 1** and enable to quantify inhomogeneities and incompatibilities. Subsequently, the relationships are reiterated in detail.

An unique deformation map $\boldsymbol{\varphi}: \boldsymbol{X} \in \mathcal{B}_0 \rightarrow \boldsymbol{x} \in \mathcal{B}_t$ requires that no closure failure along an arbitrary closed material or spatial line path, $\mathcal{C}$ or $\mathcal{C}_0$, exists. This requirement is called the integrability condition for the deformation gradient $\boldsymbol{F} := \mathrm{Grad}\,\boldsymbol{\varphi}$ and is formulated based on the Stokes theorem as

$$\oint_{\mathcal{C}} \mathrm{d}\boldsymbol{x} = \oint_{\mathcal{C}_0} \boldsymbol{F} \cdot \mathrm{d}\boldsymbol{X} = \boldsymbol{0} \quad \overset{\text{Stokes}}{\Longrightarrow} \quad \int_{\mathcal{A}_0} \mathrm{Curl}^{\mathrm{T}} \boldsymbol{F} \cdot \boldsymbol{N} \mathrm{d}A = \boldsymbol{0}. \tag{1}$$

From Eq. (1), the stronger pointwise compatibility condition follows, which ensure that no gaps or overlaps arise within the deformation of the configuration:

$$\mathrm{Curl}^{\mathrm{T}} \boldsymbol{F} \overset{!}{=} \boldsymbol{0}. \tag{2}$$

In contrast, the rotation field of purely the plastic (or elastic) part of the deformation gradient, called plastic (or elastic) dislocation density, only vanishes in case of a homogeneous deformation, but do not vanish in the presence of an inhomogeneous elasto-plastic deformation. Thus, the plastic (or elastic) dislocation density expresses the non-integrability of inhomogeneous elasto-plastic deformations. In a similar manner, the plastic (or elastic) incompatibility density, which is recaptured for additive small and multiplicative large strain plasticity in the subsequent sections, indicates incompatible plastic strains, which are responsible for residual stresses.

3.1 Small strain

In the linearized theory of small strain elasto-plasticity, the deformation gradient is approximated by $\boldsymbol{F} \approx \boldsymbol{I} + \boldsymbol{\beta}$. The displacement gradient $\boldsymbol{\beta} := \mathrm{Grad}\boldsymbol{u}$, also denoted in this context as distortion, additively decomposes into the symmetric strain tensor $\boldsymbol{\epsilon} = \frac{1}{2}[\mathrm{Grad}\boldsymbol{u} + \mathrm{Grad}^{\mathrm{T}}\boldsymbol{u}]$ and the antisymmetric rotation tensor $\boldsymbol{\omega} = \frac{1}{2}[\mathrm{Grad}\boldsymbol{u} - \mathrm{Grad}^{\mathrm{T}}\boldsymbol{u}]$, whereby both additively decompose further into elastic and plastic parts:

$$\boldsymbol{\beta} = \boldsymbol{\epsilon} + \boldsymbol{\omega} = [\boldsymbol{\epsilon}^{\mathrm{e}} + \boldsymbol{\epsilon}^{\mathrm{p}}] + [\boldsymbol{\omega}^{\mathrm{e}} + \boldsymbol{\omega}^{\mathrm{p}}] = [\boldsymbol{\epsilon}^{\mathrm{e}} + \boldsymbol{\omega}^{\mathrm{e}}] + [\boldsymbol{\epsilon}^{\mathrm{p}} + \boldsymbol{\omega}^{\mathrm{p}}] = \boldsymbol{\beta}^{\mathrm{e}} + \boldsymbol{\beta}^{\mathrm{p}} \tag{3}$$

The integrability condition guarantees:

$$\mathrm{Curl}^{\mathrm{T}} \boldsymbol{\beta} = \boldsymbol{0}. \tag{4}$$

Since the $\mathrm{Curl}\{\cdot\}$-operator is distributive,

$$\mathrm{Curl}\boldsymbol{\beta} = \mathrm{Curl}(\boldsymbol{\beta}^{\mathrm{e}} + \boldsymbol{\beta}^{\mathrm{p}}), \tag{5}$$

it follows for the plastic dislocation density

$$\boldsymbol{\alpha}^{\mathrm{p}} := \mathrm{Curl}\boldsymbol{\beta}^{\mathrm{p}} = -\mathrm{Curl}\boldsymbol{\beta}^{\mathrm{e}} \neq \boldsymbol{0} \ \text{(in general)}. \tag{6}$$

As describe above and according to the pioneering works of Kröner, see [2] among others, $\boldsymbol{\alpha}^{\mathrm{p}}$ quantifies the inhomogeneity of plastic deformations and exclusively equals to zero in case of homogeneous plastic deformations.

Furthermore, the incompatibility density tensor $\mathrm{Inc}\{\cdot\}$ with respect to the strain tensor of the total deformation requires

$$\mathrm{Inc}\boldsymbol{\epsilon} \coloneqq \mathrm{Curl}^{\mathsf{T}}\mathrm{Curl}^{\mathsf{T}}\boldsymbol{\epsilon} = \mathbf{0}, \tag{7}$$

but for its plastic and elastic parts, it yields in accordance to Eq. (6):

$$\boldsymbol{\eta}^{\mathrm{p}} \coloneqq \mathrm{Inc}\boldsymbol{\epsilon}^{\mathrm{p}} = \mathrm{Curl}^{\mathsf{T}}\mathrm{Curl}^{\mathsf{T}}\boldsymbol{\epsilon}^{\mathrm{p}} = \left[\mathrm{Curl}^{\mathsf{T}}\boldsymbol{a}^{\mathrm{p}\,\mathsf{T}}\right]^{\mathrm{sym}} = -\mathrm{Inc}\boldsymbol{\epsilon}^{\mathrm{e}} \neq \mathbf{0} \ \text{(in general)}. \tag{8}$$

Here, the plastic incompatibility density $\boldsymbol{\eta}^{\mathrm{p}}$ serves as a measure for plastic strains, which result from the non-vanishing plastic dislocation density $\boldsymbol{a}^{\mathrm{p}}$, see Eq. (6). Since $\boldsymbol{\eta}^{\mathrm{p}}$ quantifies incompatible plastic (or elastic) strains, the plastic (or elastic) incompatibility density serves as indicator for residual stresses.

Remark 1: For the sake of implementation and according to Steinmann [10] the $\mathrm{Curl}\{\cdot\}$-operation rewrites as:

$$\mathrm{Curl}\{\cdot\} = \begin{bmatrix} \{\cdot\}_{13,2} - \{\cdot\}_{12,3} & \{\cdot\}_{23,2} - \{\cdot\}_{22,3} & \{\cdot\}_{33,2} + \{\cdot\}_{32,3} \\ \{\cdot\}_{11,3} - \{\cdot\}_{13,1} & \{\cdot\}_{21,3} - \{\cdot\}_{23,1} & \{\cdot\}_{31,3} + \{\cdot\}_{33,1} \\ \{\cdot\}_{12,1} - \{\cdot\}_{11,2} & \{\cdot\}_{22,1} - \{\cdot\}_{21,2} & \{\cdot\}_{32,1} + \{\cdot\}_{31,2} \end{bmatrix}. \tag{9}$$

3.2 Large strain

According to Lee [6], the nonlinear large strain elasto-plasticity theory is based on the multiplicative decomposition of the deformation gradient into its elastic and plastic part:

$$\boldsymbol{F} = \boldsymbol{F}^{\mathrm{e}} \cdot \boldsymbol{F}^{\mathrm{p}} \tag{10}$$

As illustrated in **Figure 2**, the plastic part of the deformation gradient, $\boldsymbol{F}^{\mathrm{p}}$, represents the deformation due to the motion of dislocations (depicted as red circles) in the periodically arranged crystal lattice. The lattice orientation remains unchanged in the plastic intermediate configuration $\overline{\mathcal{B}}$. The elastic part $\boldsymbol{F}^{\mathrm{e}}$ then causes the corresponding lattice distortion.

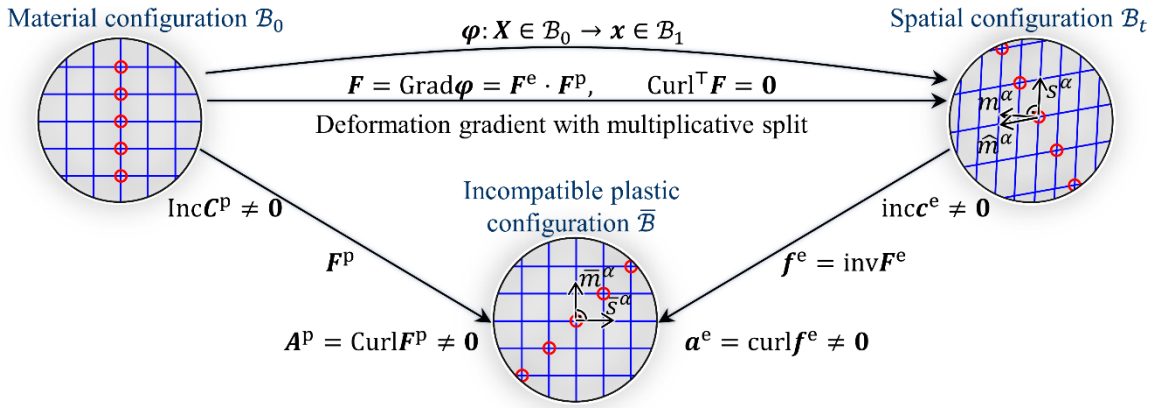

Figure 2: Multiplicative elasto-plasticity modelling includes an incompatible plastic intermediate configuration

Remark 4: Within multiplicative modelling, purely the elastic part of the deformation transforms the slip systems. The elastic part of the deformation gradient and the left Cauchy Green Tensor, $\boldsymbol{F}^{\mathrm{e}}$ and $\boldsymbol{b}^{\mathrm{e}} = \boldsymbol{F}^{\mathrm{e}} \cdot \boldsymbol{F}^{\mathrm{e}\mathsf{T}}$, allow to compute the slip direction $\boldsymbol{s}^{\alpha}$ and the slip plane normal $\boldsymbol{m}^{I}$ in the spatial configuration in dependency of their counterparts in the plastic intermediate configuration: $\boldsymbol{s}^{\alpha} = \boldsymbol{F}^{\mathrm{e}} \cdot \bar{\boldsymbol{s}}^{\alpha}$, $\hat{\boldsymbol{m}}^{\alpha} = \boldsymbol{b}^{\mathrm{e}} \cdot \boldsymbol{m}^{\alpha}$ and $\boldsymbol{m}^{\alpha} = \boldsymbol{F}^{\mathrm{e}-\mathsf{T}} \cdot \bar{\boldsymbol{m}}^{\alpha}$. The transformation of a slip system is additionally depicted in **Figure 2**.

Plastic and elastic dislocation density

The rotation field with respect to the plastic part of the deformation gradient, which is again denoted as plastic dislocation density, is defined as:

$$\boldsymbol{A}^{\mathrm{p}} := \mathrm{Curl}\boldsymbol{F}^{\mathrm{p}} \neq \boldsymbol{0} \text{ (in general).} \tag{11}$$

In accordance to the additive small strain theory, $\boldsymbol{A}^{\mathrm{p}}$ differs from zero in case of inhomogeneous plastic deformations. Thus, the plastic intermediate configuration $\overline{\mathcal{B}}$ is in general incompatible and the plastic dislocation density $\boldsymbol{A}^{\mathrm{p}}$ is directly linked to the GNDs, which arise during inhomogeneous plastic deformations. An incompatible plastic configuration induces incompatible elastic distortions to guarantee the continuity of the continuum. Therefore, it follows for the counterparts in the elastic regime:

$$\boldsymbol{a}^{\mathrm{e}} := \mathrm{curl}\boldsymbol{f}^{\mathrm{e}} \neq \boldsymbol{0} \text{ (in general).} \tag{12}$$

The relationship between the elastic and plastic dislocation density, $\boldsymbol{A}^{\mathrm{p}}$ and $\boldsymbol{a}^{\mathrm{e}}$, which is proposed [5] and further extensively investigated by Cermelli and Gurtin [7], results in:

$$\frac{1}{\det\boldsymbol{F}^{\mathrm{p}}}\boldsymbol{F}^{\mathrm{p}} \cdot \boldsymbol{A}^{\mathrm{p}} = \frac{1}{\det\boldsymbol{f}^{\mathrm{e}}}\boldsymbol{f}^{\mathrm{e}} \cdot \boldsymbol{a}^{\mathrm{e}}. \tag{13}$$

Remark 2: The plastic dislocation density $\boldsymbol{A}^{\mathrm{p}}$ provides further background information: Its diagonal entries arise with the occurrence of screw dislocations, whereby non-diagonal entries are linked with edge dislocations. In addition, a multiplication with a direction vector $\boldsymbol{t}$ of an assumed dislocation line leads to the associated Burgers vector $\boldsymbol{b}$, which describes the closure failure: $\boldsymbol{b} = \boldsymbol{A}^{\mathrm{p}\top} \cdot \boldsymbol{t}$.

Remark 3: The plastic part of the deformation gradient, $\boldsymbol{F}^{\mathrm{p}}$, which is necessary for the computation of the plastic dislocation density $\boldsymbol{A}^{\mathrm{p}}$, is only accessible if crystal plasticity modelling is applied. Unfortunately, in commonly used commercial FE software packages, for example *Marc/Mentat* or *Abaqus*, only a phenomenological multiplicative approach for large strain plasticity as described in Simo and Hughes [8] is implemented and so, the plastic part of the deformation gradient remains still unknown. However, a possible option to incorporate crystal plasticity modelling in the above mentioned FE packages is the usage of the *Fortran* library *DAMASK* [9].

Plastic and elastic incompatibility density

The compatibility relations and their correlations with dislocation densities within the linear theory of small strains, see Kröner [2], are extended by Steinmann [4] to the general nonlinear case of large strains. Applying the multiplicative large strain modelling, the incompatibilities of the continuum rotations contained in $\boldsymbol{F}^{\mathrm{e}} = \mathrm{inv}\boldsymbol{f}^{\mathrm{e}}$ lead to stress-free lattice curvatures, while the incompatibilities of the elastic part of the left Cauchy-Green strain tensor $\boldsymbol{b}^{\mathrm{e}}$ cause the lattice distorsions, which result in residual stresses.

The theories of differential geometry is exploited in [4] to show that the non-integrability of plastic and elastic strains metrics $\boldsymbol{C}^{\mathrm{p}}$ (plastic part of the right Cauchy-Green tensor) and $\boldsymbol{c}^{\mathrm{e}} = \mathrm{inv}\boldsymbol{b}^{\mathrm{e}}$ (elastic part of the left Cauchy-Green tensor) coincides with the non-vanishing plastic and elastic Riemann curvatures $\boldsymbol{H}^{\mathrm{p}}$ and $\boldsymbol{h}^{\mathrm{e}}$. According to these considerations, the plastic incompatibility density (in Euclidean space) is computed by,

$$2\boldsymbol{H}^{\mathrm{p}} = \mathrm{Ink}\boldsymbol{C}^{\mathrm{p}} \coloneqq \mathrm{Curl}^{\mathsf{T}}\mathrm{Curl}^{\mathsf{T}}\boldsymbol{C}^{\mathrm{p}} + \{\mathrm{Grad}\boldsymbol{C}^{\mathrm{p}}\}\bowtie\{\mathrm{Grad}\boldsymbol{C}^{\mathrm{p}}\} \neq \boldsymbol{0}\ (\text{in general}), \tag{14}$$

whereby $\{\cdot\}\bowtie\{\cdot\}$ describes a special product of third-order tensors, see the implementation guidance in the subsection 3.3. Analogously, it follows for the elastic regime,

$$-2\boldsymbol{h}^{\mathrm{e}} = \mathrm{ink}\boldsymbol{c}^{\mathrm{e}} \coloneqq \mathrm{curl}^{\mathsf{T}}\mathrm{curl}^{\mathsf{T}}\boldsymbol{c}^{\mathrm{e}} + \{\mathrm{grad}\boldsymbol{c}^{\mathrm{e}}\}\bowtie\{\mathrm{grad}\boldsymbol{c}^{\mathrm{e}}\} \neq \boldsymbol{0}\ (\text{in general}). \tag{15}$$

As in small strain plasticity, the plastic and elastic incompatibility densities are a measure for the incompatibility of the plastic strains and their elastic counterparts. Since the latter cause residual strains, both incompatibility densities are suited as residual stress indicators.

Remark 5: In commercial FE-software packages, for example *Marc/Mentat* or *Abaqus*, access to the elastic part of the left Cauchy-Green tensor, $\boldsymbol{b}^{\mathrm{e}}$, is provided via subroutines in case of using their phenomenological large strain plasticity modelling. The plastic part of the right Cauchy-Green tensor then follows with $\boldsymbol{C}^{\mathrm{p}} = \boldsymbol{F}^{\mathsf{T}} \cdot \mathrm{inv}\boldsymbol{b}^{\mathrm{e}} \cdot \boldsymbol{F}$. Consequently, the plastic and elastic incompatibility densities, $\mathrm{Inc}\boldsymbol{C}^{\mathrm{p}}$ and $\mathrm{inc}\boldsymbol{c}^{\mathrm{e}}$ – indicators for residual stresses, are even computable without using crystal plasticity.

A relation between the elastic and plastic incompatibility densities, see Eq. (14) and (15), is derived in Steinmann [4] as:

$$\frac{\det\left(\boldsymbol{F}^{\mathrm{p}^{-1}}\right)}{\det\boldsymbol{F}^{\mathrm{p}}}\boldsymbol{F}^{\mathrm{p}} \cdot \boldsymbol{H}^{\mathrm{p}} \cdot \boldsymbol{F}^{\mathrm{p}^{\mathsf{T}}} = \frac{\det\left(\boldsymbol{f}^{\mathrm{e}^{-1}}\right)}{\det\boldsymbol{f}^{\mathrm{e}}}\boldsymbol{f}^{\mathrm{e}} \cdot \boldsymbol{h}^{\mathrm{e}} \cdot \boldsymbol{f}^{\mathrm{e}^{\mathsf{T}}} \tag{16}$$

Unfortunately, Eq. (16) again requires an access to the plastic and elastic deformation gradient, respectively.

3.3 An implementation scheme for the plastic incompatibility density

While in the previous subsection focus is put on the relationships between the plastic and elastic dislocation and incompatibility densities, some hints for implementation are given subsequently.

Computation of the plastic incompatibility density from Riemann curvatures

The steps to compute the incompatibility density is described for the plastic regime, whereby Einstein summation is used as in [4].

After differentiation of the plastic part of the Cauchy Green tensor, $\boldsymbol{C}^{\mathrm{p}}$, with respect to the material coordinates $\boldsymbol{X}$, the plastic Riemann connection is achieved by

$$\mathcal{M}^{\mathrm{p}}_{IJK}(\boldsymbol{C}^{\mathrm{p}}) := \tfrac{1}{2}\left[C^{\mathrm{p}}_{IJ,K} - C^{\mathrm{p}}_{JK,I} + C^{\mathrm{p}}_{KI,J}\right] \tag{17}$$

Next, the plastic material Riemann curvature tensor is computed, whereby differentiation of the Riemann connection $\mathcal{M}^{\mathrm{p}}_{IJK}$, again with respect to the material coordinates $\boldsymbol{X}$, is required:

$$M^{\mathrm{p}}_{IJKL}(\boldsymbol{C}^{\mathrm{p}}) := -2\left[\mathcal{M}^{\mathrm{p}}_{IJK,L} + \mathcal{M}^{\mathrm{p}}_{AIK}\mathcal{M}^{\mathrm{p}\,A}_{\ \ JL}\right]. \tag{18}$$

Finally, the plastic incompatibility tensor is obtained by

$$H^{\mathrm{p}MN}(\boldsymbol{C}^{\mathrm{p}}) \coloneqq -\tfrac{1}{4}\mathcal{E}^{MIJ}M^{\mathrm{p}}_{IJKL}\mathcal{E}^{KLN} = \tfrac{1}{2}\mathcal{E}^{MIJ}\mathcal{M}^{\mathrm{p}}_{IJK,L}\mathcal{E}^{KLN} + \tfrac{1}{2}\mathcal{E}^{MIJ}\mathcal{M}^{\mathrm{p}}_{AIK}\mathcal{M}^{\mathrm{p}\,A}_{\ \ JL}\mathcal{E}^{KLN}, \tag{19}$$

whereby $\mathcal{E}$ refers to the third-order Levi-Cita-Symbol with

$$\mathcal{E}^{123} = \mathcal{E}^{231} = \mathcal{E}^{321} = 1, \;\; \mathcal{E}^{132} = \mathcal{E}^{321} = \mathcal{E}^{231} = -1 \tag{20}$$

and 0 else. Within Euclidean space the first term in Eq. (19) equals

$$\mathcal{E}^{MIJ}\mathcal{M}^{\mathrm{p}}_{IJK,L}\mathcal{E}^{KLN} = \mathrm{Curl}^{\mathsf{T}}\mathrm{Curl}^{\mathsf{T}}\boldsymbol{C}^{\mathrm{p}}, \tag{21}$$

whereas the second term in Eq. (19) can be formulated as

$$\mathcal{E}^{MIJ}\mathcal{M}^{\mathrm{p}}_{AIK}\mathcal{M}^{\mathrm{p}\,A}_{\;\;JL}\mathcal{E}^{KLN} = \{\mathrm{Grad}\boldsymbol{C}^{\mathrm{p}}\}\bowtie\{\mathrm{Grad}\boldsymbol{C}^{\mathrm{p}}\}. \tag{22}$$

Thus, Eq. (14) follows from Eq. (19). The computation of the elastic incompatibility density $\mathrm{ink}\boldsymbol{c}^{\mathrm{e}}$ from the elastic part of the left Cauchy Green tensor works in an analogous way. For further details, the interested reader is referred to [4].

Remark 6: For the sake of implementation and according to Kaiser and Menzel [10] the $\mathrm{Curl}^{\mathsf{T}}\mathrm{Curl}^{\mathsf{T}}\{\cdot\}$-operation rewrites as:

$$\begin{aligned}\mathrm{Curl}^{\mathsf{T}}\mathrm{Curl}^{\mathsf{T}}\{\cdot\} \;=\; &\begin{bmatrix}\{\cdot\}_{12,12}+\{\cdot\}_{13,13} & \{\cdot\}_{11,21}+\{\cdot\}_{13,23} & \{\cdot\}_{11,31}+\{\cdot\}_{12,32}\\ \{\cdot\}_{22,12}+\{\cdot\}_{23,13} & \{\cdot\}_{21,21}+\{\cdot\}_{23,23} & \{\cdot\}_{21,31}+\{\cdot\}_{22,32}\\ \{\cdot\}_{32,12}+\{\cdot\}_{33,13} & \{\cdot\}_{31,21}+\{\cdot\}_{33,23} & \{\cdot\}_{31,31}+\{\cdot\}_{32,32}\end{bmatrix}\\ -\;&\begin{bmatrix}\{\cdot\}_{11,22}+\{\cdot\}_{11,33} & \{\cdot\}_{12,11}+\{\cdot\}_{12,33} & \{\cdot\}_{13,11}+\{\cdot\}_{13,22}\\ \{\cdot\}_{21,22}+\{\cdot\}_{21,33} & \{\cdot\}_{22,11}+\{\cdot\}_{22,33} & \{\cdot\}_{23,11}+\{\cdot\}_{23,22}\\ \{\cdot\}_{31,22}+\{\cdot\}_{31,33} & \{\cdot\}_{32,11}+\{\cdot\}_{32,33} & \{\cdot\}_{33,11}+\{\cdot\}_{33,22}\end{bmatrix}.\end{aligned} \tag{23}$$

Differentiation of quadrature point quantities

For the differentiation of quadrature point quantities – for example the tensor components $C^{\mathrm{p}}_{IJ,K}$ within $\mathrm{Grad}\boldsymbol{C}^{\mathrm{p}}$ – a two-step technique is applied as already proposed in Steinmann [5] for a post-processing approach with respect to the plastic dislocation density:

Firstly, the tensor components are mapped from the quadrature points to the discretization nodes, see **Figure 3 a**. Therefore, the *Superconvergent Patch Recovery Procedure* (*SPR*) [11] as an alternative to the *global L^2-smoothing* [12] is applied. The mapped tensor quantities at each discretization node are indicated in the following by a tilde.

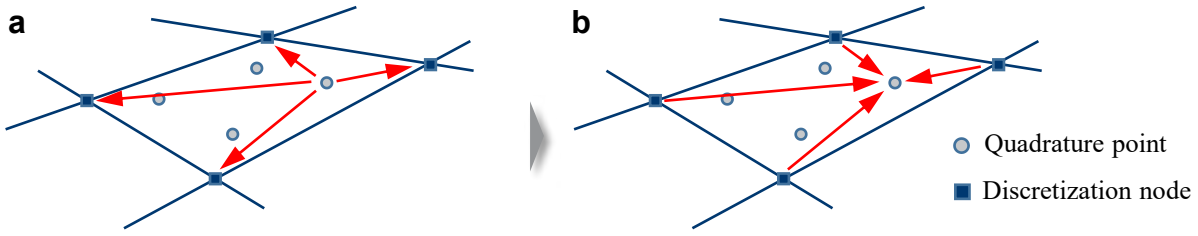

Extrapolation via patch-recovery **Differentiation** via shape functions

Figure 3: A two-step technique for the differentiation of integration point quantities

Secondly, as illustrated in **Figure 3 b**, the differentiation of a tensor component is evaluated at quadrature points by the help of shape functions:

$$\mathrm{Grad}\boldsymbol{C}^{\mathrm{p}\,j} = \sum_{a=1}^{n_{\mathrm{en}}} \left[\widetilde{\boldsymbol{C}}^{\mathrm{p}\,a} \otimes \frac{\partial N^a(\xi^j)}{\partial \xi}\right] \cdot \left[\boldsymbol{X}^a \otimes \frac{\partial N^a(\xi^j)}{\partial \xi}\right]^{-1}, \tag{24}$$

whereby j refers to the quadrature point, a refers to the elementwise discretization node, n_{en} denotes the number of element nodes and $N(\boldsymbol{\xi})$ refers to the shape functions with respect to its natural coordinates.

4 COMPUTATIONAL EXAMPLES

The functional principle of the plastic incompatibility density $\mathrm{Inc}\boldsymbol{C}^{\mathrm{p}}$ as an accompanying indicator for residual stresses during forming simulations is demonstrated for two examples of a homogeneous and an inhomogeneous elastoplastic deformation.

As a representative of FE-packages with phenomenological, multiplicative large strain plasticity modelling, *Marc/Mentat* is used for both examples. Here, the deformation gradient $\boldsymbol{F}$ and the elastic part of left Cauchy Green tensor, $\boldsymbol{b}^{\mathrm{e}}$, are accessible for each quadrature point through subroutines. The plastic part of the right Cauchy Green tensor then follows as:

$$\boldsymbol{C}^{\mathrm{p}} = \boldsymbol{F}^{\mathrm{T}} \cdot \boldsymbol{c}^{\mathrm{e}} \cdot \boldsymbol{F} \qquad \text{with} \quad \boldsymbol{c}^{\boldsymbol{e}} = \mathrm{inv}\boldsymbol{b}^{\mathrm{e}} \tag{25}$$

The plastic incompatibility density as in Eq. (14) is then computed according to the techniques presented in subsection 3.3.

The same elasto-plastic material modelling is applied in both examples. The elastic constants are set to $E = 210.000$ MPa and $\nu = 0.3$. The isotropic plastic hardening, which is modelled by the Hockett-Sherby function with respect to the equivalent plastic strain $\bar{\epsilon}^{\mathrm{p}}$, is used as follows:

$$\sigma_{\mathrm{yield}}(\bar{\epsilon}^{\mathrm{p}}) = 185.2 + [577.1 - 185.2]\left[1 - \exp\left(-2.18\bar{\epsilon}^{\mathrm{p}\,0.667}\right)\right] \tag{26}$$

4.1 Example for homogeneous elasto-plastic deformation: Tension

As the first example, an elasto-plastic deformation by a pure tension is considered. In a two-dimensional model, a bar (height: 180 mm, length: 200 mm) is drawn force-controlled in e_1-direction until an enlargement of 100 mm is reached, see **Figure 1 a**. The resulting constant Cauchy stress equals to 473 MPa (v.Mises coincides with the 11-component) in the fully loaded stated and the equivalent plastic strain computes to 0.47. After reducing the loading back to zero, also the stresses vanish. Thus, no residual stresses are generated. In accordance, since tension leads to a purely homogeneous deformation, the plastic incompatibility density also remains zero through all stages, see **Figure 1 b**.

4.2 Example for inhomogeneous elasto-plastic deformation: Bending

Pure bending, as a benchmark for an inhomogeneous deformation, is considered in the second example. The two-dimensional model consists of a bar (height: 40 mm, length: 150 mm) and is bended by a punch with a travel way of 50 mm, see **Figure 5 a**. The maximal Cauchy stress is computed to 474 MPa (v.Mises) when fully loaded and equivalent plastic strains are computed up to maximal 0.48. When the punch is removed, the stresses reduces only to 437 MPa. The remaining stresses are residual stresses, which are generated through the inhomogeneous plastic deformation. In contrast to the previous examples, the plastic incompatibility density arises (during forming) to a maximum of 0.42 in the L^2-norm when

fully loaded. Thus, the plastic incompatibility density indicates the generation of residual stresses even during forming and despite application of external loading, see **Figure 5 b**.

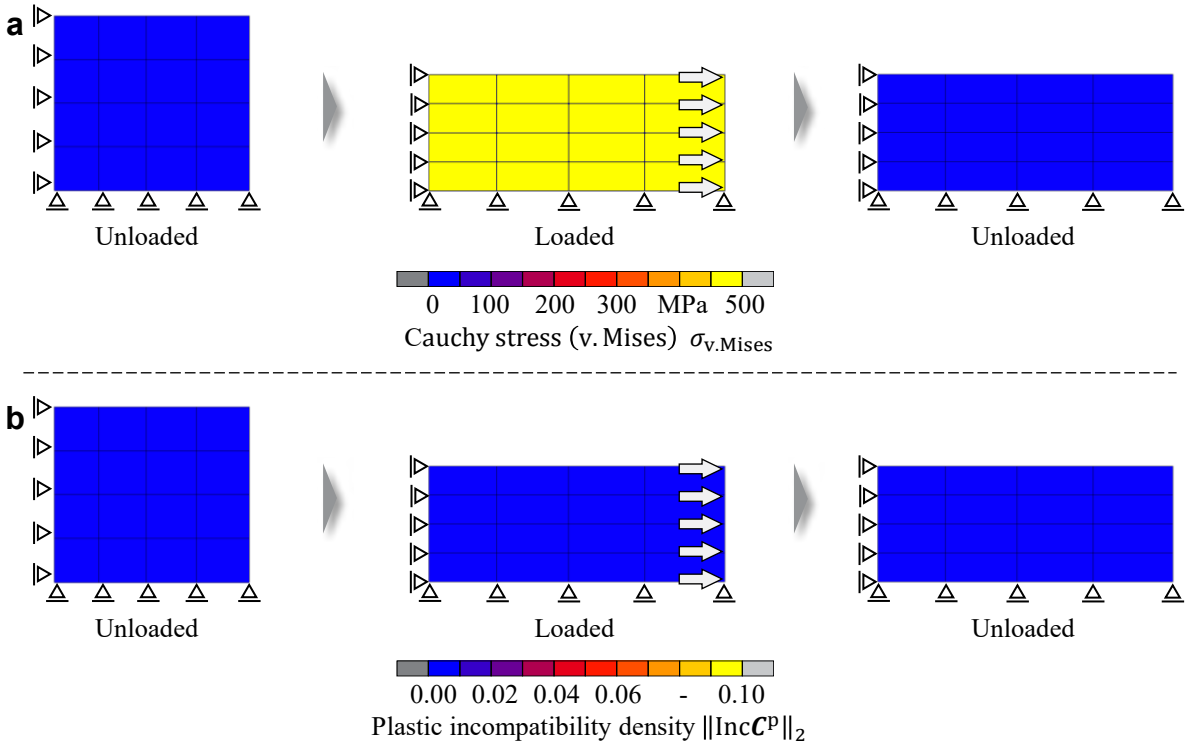

Figure 4: No plastic incompatibility density is computed within a homogeneous deformation

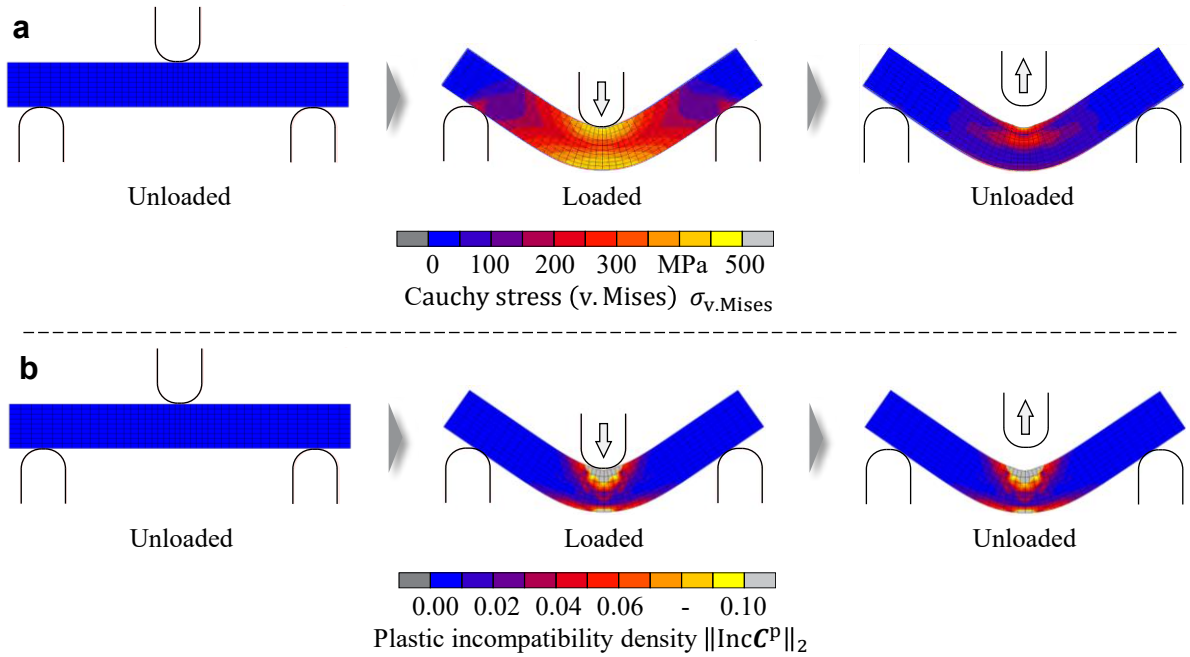

Figure 5: Plastic incompatibility density arise during forming in case of an inhomogeneous deformation

5 CONCLUSION

Residual stresses are of major interest in manufacturing of functional components. However, the generation of residual stresses is not able to be tracked during forming. Typically, purely the remaining stress state after removing all external loads is investigated. However, residual stresses are the result of incompatible plastic strains in case of an inhomogeneous plastic deformation. Further, the plastic dislocation density measures the incompatibility of the plastic intermediate configuration. Thus, the plastic and elastic dislocation and incompatibility densities are exploited to indicate the generation of residual stresses even during the application of external loadings. Theoretical aspects regarding dislocation and incompatibility densities in small and large strain plasticity are reiterated and hints for implementation are provided. Two examples with a homogeneous and an inhomogeneous plastic deformation demonstrated the functionality of the indicators.

ACKNOWLEDGMENT

Our research activities are funded by the *Deutsche Forschungsgemeinschaft* (*DFG*) within the scope of the priority program *SPP2013 - P10* (project number: 374688875).

REFERENCES

[1] Tekkaya, A.E. and Gerhardt, J. *Residual Stresses in Cold-Formed Workpieces*. Annals of the CIRP (1985), **34-1**:225-230.

[2] Kröner, E.: *Allgemeine Kontinuumstheorie der Versetzungen und Eigenspannungen*. Arch. Ration. Mech. Anal., (1959), **4-1**:273-334.

[3] Kröner, E. and Seeger, A. *Nichtlineare Elastizitätstheorie der Versetzungen und Eigenspannungen.* Arch. Rat. Mech. Anal., (1959) **3**:97–119.

[4] Steinmann, P. *Geometrical Foundations of Continuum Mechanics: An Application to First- and Second-Order Elasticity and Elasto-Plasticity*. Berlin: Springer Verlag (2015).

[5] Steinmann, P. *Modellierung und Numerik duktiler kristalliner Werkstoffe*. Forschungs- und Seminarberichte aus dem Bereich der Mechanik der Universität Hannover, Bericht **F97/1**, Habilitationsschrift, (1996).

[6] Lee, E.H. *Elastic-plastic deformations at finite strains*. J. Appl. Mech., (1969) **36**:1-6.

[7] Cermelli, P. and Gurtin, M.E. *Geometrically necessary dislocations in finite plasticity*. J. Mech. Phys. Solids, (2000) **49**:1539-1568.

[8] Simo, J.C. and Hughes, T.J.R. *Computational Inelasticity*. New York: Springer (1998).

[9] Roters, F. and Eisenlohr, P. and Kords, C. and Tjahjanto, D.D. and Diehl, M. and Raabe, D. *DAMASK: Düsseldorf Advanced Material Simulation Kit for studying crystal plasticity using an FE based or a spectral numerical solver*, Procedia IUTAM, (2012) **3**:3-10.

[10] Kaiser, T. and Menzel, A. *An incompatibility tensor-based gradient plasticity formulation - theory and numerics.* Comp. Methods Appl. Mech. Eng., (2019) **345**:671-700.

[11] Zienkiewicz, O.C. and Zhu, J.Z. *The superconvergent patch recovery and a posteriori error estimates. Part 1: the recovery technique*. Int. J. Numer. Methods Eng., (1992) **33**:1331-1364.

[12] Hinton, E. and Campbell, J.S. *Local and global smoothing of discontinuous finite element functions using a least-squares method.* Int. J. Numer. Methods Eng., (1974) **3**:461-480.